The thesis committee for Erik John Brugamyer certifies
that this is the approved version of the following thesis

Silicon and Oxygen Abundances in Planet-Host Stars

APPROVED BY

SUPERVISING COMMITTEE:

Sarah E. Dodson-Robinson, Supervisor

Eiichiro Komatsu

Silicon and Oxygen Abundances in Planet-Host Stars

by

Erik John Brugamyer, B.A.; B.S.; M.P.A.

THESIS

Presented to the Faculty of the Graduate School of

The University of Texas at Austin

in Partial Fulfillment

of the Requirements

for the Degree of

Master of Arts

THE UNIVERSITY OF TEXAS AT AUSTIN

December 2010

To Rebeca

Acknowledgments

I would like to thank Sally Dodson-Robinson, my supervisor for this project. Her patience, insight, suggestions and financial support have all been most welcome. She helped take a rough idea and shape it into the present focused paper.

I would also like to thank Bill Cochran, who provided many of the spectra used in this analysis. As an advisor for this project, Bill trained me on the 2.7m telescope and the data reduction process. I have always found his door open for many questions and tips on handling high resolution stellar spectroscopic data.

Finally, I would like to thank Chris Sneden, my long-time unofficial mentor. I have used Chris' MOOG software for the spectroscopic analysis – an invaluable tool without which the present research would not have been possible. More importantly, Chris has long served as a role model and caring mentor.

Silicon and Oxygen Abundances in Planet-Host Stars

Erik John Brugamyer, M.A.
The University of Texas at Austin, 2010

Supervisor: Sarah E. Dodson-Robinson

The positive correlation between planet detection rate and host star iron abundance lends strong support to the core accretion theory of planet formation. However, iron is not the most significant mass contributor to the cores of giant planets. Since giant planet cores grow from silicate grains with icy mantles, the likelihood of gas giant formation should depend heavily on the oxygen and silicon abundance of the planet formation environment. Here we compare the silicon and oxygen abundances of a set of 60 planet hosts and a control sample of 60 metal-rich stars without giant planets. We find a 99% probability that planet detection rate depends on the silicon abundance of the host star, over and above the observed planet-metallicity correlation. Due to our large error bars on oxygen abundances, we do not yet observe any correlation between oxygen abundance and planet detection rate. We predict that a correlation between planet occurrence and oxygen abundance should emerge when we can measure [O/Fe] at 0.05 dex precision. Since up to 20%

of the carbon in the universe may be in refractory grains, we also predict that planet detection rate should correlate positively with host star carbon abundance for any population of planets formed by core accretion.

Table of Contents

Chapter 1

Introduction

The tendency for planets to orbit metal-rich stars lends strong support to the core accretion model of planet formation, whereby planets grow through accretion of solid, metal-rich material to form massive cores. Within the context of core accretion (cf. Safronov & Zvjagina 1969; Pollack et al. 1996), heavy element abundances are important to the extent that they contribute to the inventory of solid material available for planetesimal formation. Iron (the typically-used proxy for overall metallicity) is certainly an important component, but there are other more significant contributors, especially oxygen, silicon and carbon.

Oxygen is thought to be the single most important contributor to the mass of giant planets, primarily via water ice accreted beyond the snow line of the disk (Hayashi 1981, Weidenshilling 1977) and, to a lesser extent, through the oxides of Si, Mg, Ca, and Al. Carbon, via heavy organic compounds, is probably the second most important mass contributor (Lodders 2004), followed by silicon. These elements often demonstrate different abundance patterns relative to iron. Robinson et al. (2006) reported relative silicon and nickel enrichment in planet hosts and Fuhrmann & Bernkopf (2008) have reported enhancements in alpha-capture elements. Thus, for purposes of planet-formation, iron is likely not an ideal proxy for overall metallicity.

Previous tests of how individual elements contribute to planet formation have focused on the possibility that planet hosts are chemically peculiar stars with abundance ratios quite different from typical Population I stars. If planet hosts are chemically peculiar, the slopes of [X/Fe] vs. [Fe/H] among planet hosts should be distinct from what Galactic chemical enrichment models (e.g. Timmes et al. 1995) predict. Bodaghee et al. (2003) found no such differences in their sample for alpha- and iron-peak elements. For a given value of [Fe/H], they observe no difference in the trends of [X/Fe] between the two groups of stars. Stars with planets therefore appear to be indistinguishable from other field stars, and seem to simply lie on the high-metallicity end of otherwise "normal" stellar distributions.

The present analysis is aimed at examining the most abundant heavy elements important for planet formation. We have chosen to focus first on silicon and oxygen. Our hypothesis is that if core-accretion is responsible for the majority of known giant planets, then for a given [Fe/H] their stellar hosts should show enhancements in silicon and oxygen relative to iron. We therefore wish to determine whether there is a statistically-significant difference in the silicon and oxygen abundance distributions of stars with planets, compared to those without any known planets.

Chapter 2

Observations and Data Reduction

For this study, we selected 60 FGK host stars and 60 non-host stars for comparison. All non-host stars were selected from the ∼300 stars being monitored as part of the McDonald Observatory Planetary Search program (hereafter "MOPS"; see Wittenmyer et al. 2006 for a description of the program and detection limits). Using the current instrumental configuration ("Phase III"; begun in 1998), the program achieves routine internal precision of 6–9 m s^{-1}. With a monitoring baseline of over 10 years, we can thus exclude roughly Jupiter-mass companions out to 5 AU, or roughly Neptune-mass companions out to 1 AU, around these stars. Fifteen of our planet-host stars were also selected from this same program. The remaining hosts were observed independently by E.B.

Our host stars were selected in a statistically haphazard manner, based on the highest-resolution data available from the MOPS program, or on what was available for observation during our supplemental observing runs. Since these stars are naturally more metal-rich, we also chose the most metal-rich stars available from the MOPS program for our non-host sample. This was done by cross-referencing the MOPS list with available metallicity references from the SIMBAD Astronomical Database[1] and the NASA/IPAC/NExScI Star and Exoplanet Database ("NStED")[2] and choosing non-host stars in such a manner that the overall metallicity distributions of our two samples were as similar as possible.

The data were obtained between July 1998 and January 2010 on the 2.7m Harlan J. Smith and Hobby-Eberly telescopes at the McDonald Observatory of The University of Texas at Austin. For the 2.7m telescope, we utilized the 2dcoudé cross-dispersed echelle spectrograph (Tull et al. 1994). The spectrograph uses a 2048x2048 Tektronix CCD with 24 μm pixels and our configuration uses the "E2" grating with 52.67 gr mm^{-1}. With a 1.2 arcsec slit, we achieve a resolution ($=\lambda/\Delta\lambda$) of R=60,000 in this configuration. The wavelength coverage extends from 3750 Å to 10,200 Å. Coverage is complete from the blue end to 5691 Å, with increasingly large inter-order gaps thereafter. The signal-to-noise ratio of our data range from ~100-500.

The data were reduced using standard routines within the *echelle* and *onedspec* packages of the Image Reduction and Analysis Facility (IRAF). The process included overscan trimming, bias frame subtraction, removal of scattered light, flat field division, extraction of the orders and wavelength calibration (using a ThAr calibration lamp spectrum). We then manually removed any cosmic rays that IRAF's interpolation routines were unable to handle. The final steps were removal via division of the blaze function, normalization

---

[1] http://simbad.u-strasbg.fr/simbad/

[2] http://nsted.ipac.caltech.edu/

of the continuum and combining orders.

Chapter 3

Measuring Abundances

3.1 Atmospheric parameters and iron abundances

All stellar parameters and abundances were determined using MOOG (Sneden 1973) – a local thermodynamic equilibrium (LTE) line analysis and spectrum synthesis code – and a grid of Kurucz (1993a) ATLAS9 model atmospheres. We constrained the stellar parameters of our targets using a carefully-selected list of 65 isolated, unblended neutral iron lines and 22 singly-ionized iron lines, spanning a wide range in excitation potentials and equivalent widths. The equivalent widths of each of these lines was measured in our program stars using an Interactive Data Language (IDL) routine written exclusively for this purpose. The program fits either a gaussian or voigt profile to each line, and allows for manual adjustment of the continuum. The program output is a list of equivalent widths for use with MOOG.

MOOG calculates a curve of growth for a particular species and, using the input atomic line parameters (wavelength, excitation potential and oscillator strength), force-fits abundances to match the measured equivalent widths for each line. Our Fe I line parameters, including oscillator strengths (or "log *gf*" values), were taken from the National Institute of Standards and

Technology (NIST) Atomic Spectra Database[1], supplemented with values from O'Brian et al. (1991). See Table 3.1 for the full list of neutral iron lines used in our analysis. Our Fe II parameter values were taken from Meléndez & Barbuy (2009) and are listed in Table 3.2.

---

[1] available at http://www.nist.gov/physlab/data/asd.cfm

Table 3.1. List of Fe I lines

Wavelength (Angstroms)	Excitation Potential (eV)	Oscillator Strength (log *gf*)	Solar Equivalent Width (mÅ)
4445.47	0.09	-5.38	44.5
4537.67	3.27	-2.88	19.6
4556.93	3.25	-2.69	28.2
4593.54	3.94	-2.06	30.4
4788.75	3.24	-1.76	69.5
4873.75	3.30	-3.06	12.8
5123.72	1.01	-3.06	116.6
5127.68	0.05	-6.12	22.5
5151.91	1.01	-3.32	105.1
5213.81	3.94	-2.76	6.5
5247.05	0.09	-4.98	72.4
5250.21	0.12	-4.90	75.4
5295.30	4.42	-1.69	28.4
5373.70	4.47	-0.87	65.6
5386.34	4.15	-1.77	32.9
5560.21	4.43	-1.19	51.9
5577.03	5.03	-1.55	13.0
5636.70	3.64	-2.61	21.4
5705.47	4.30	-1.60	38.5
5753.12	4.26	-0.69	87.6
5778.45	2.59	-3.59	21.6
5811.92	4.14	-2.43	10.6
5814.81	4.28	-1.97	22.1
5849.68	3.69	-2.99	7.5
5858.78	4.22	-2.26	13.2
5927.79	4.65	-1.09	44.3
5956.69	0.86	-4.50	57.6
6034.03	4.31	-2.42	8.8
6120.24	0.92	-5.95	5.6
6151.62	2.18	-3.37	51.2
6159.37	4.61	-1.97	11.7
6165.36	4.14	-1.47	46.2
6187.99	3.94	-1.72	48.5
6226.73	3.88	-2.20	29.8
6265.13	2.18	-2.54	92.5
6380.75	4.19	-1.38	55.5
6392.54	2.28	-4.03	17.8
6498.94	0.96	-4.69	46.7
6509.61	4.08	-2.98	3.6
6591.33	4.59	-2.06	10.5
6593.87	2.43	-2.37	90.7
6597.56	4.79	-1.06	42.8
6608.02	2.28	-4.04	18.3
6609.11	2.56	-2.66	72.5
6646.93	2.61	-3.99	11.0
6667.42	2.45	-4.40	5.6
6667.73	4.58	-2.15	9.6

Table 3.1 (cont'd)

Wavelength (Angstroms)	Excitation Potential (eV)	Oscillator Strength (log gf)	Solar Equivalent Width (mÅ)
6699.16	4.59	-2.18	8.5
6703.57	2.76	-3.15	37.4
6704.48	4.22	-2.66	5.7
6710.32	1.49	-4.87	16.1
6725.35	4.10	-2.30	17.6
6732.07	4.58	-2.21	6.8
6739.52	1.56	-4.94	11.0
6745.09	4.58	-2.17	9.1
6745.95	4.08	-2.76	6.3
6746.95	2.61	-4.35	4.8
6753.47	4.56	-2.28	6.2
6837.02	4.59	-1.80	17.7
6839.83	2.56	-3.45	32.3
6843.65	4.55	-0.93	65.5
6851.63	1.61	-5.31	5.4
6857.24	4.08	-2.16	22.4
6862.49	4.56	-1.57	30.7
6978.85	2.48	-2.45	88.3

Table 3.2. List of Fe II lines

Wavelength (Angstroms)	Excitation Potential (eV)	Oscillator Strength (log gf)	Solar Equivalent Width (mÅ)
4413.60	2.68	-3.79	39.9
4491.40	2.86	-2.71	80.0
4582.84	2.84	-3.18	61.7
4620.52	2.83	-3.21	62.9
5132.67	2.81	-4.08	24.9
5197.58	3.23	-2.22	89.6
5234.62	3.22	-2.18	91.4
5264.81	3.23	-3.13	48.0
5325.55	3.22	-3.16	48.2
5414.07	3.22	-3.58	31.7
6084.11	3.20	-3.79	21.1
6149.26	3.89	-2.69	39.6
6247.56	3.89	-2.30	57.3
6369.46	2.89	-4.11	20.7
6383.72	5.55	-2.24	9.4
6416.92	3.89	-2.64	43.2
6446.41	6.22	-1.97	4.5
6516.08	2.89	-3.31	62.1
7222.39	3.89	-3.26	19.6
7224.49	3.89	-3.20	24.9
7515.83	3.90	-3.39	14.8
7711.72	3.90	-2.50	53.5

3.1.1 Calibration using the Solar spectrum

We began the analysis by measuring iron line equivalent widths in a spectrum of the daytime sky, taken through the solar port of the 2.7m telescope. Figure 3.1 shows the results of these measurements, by plotting the derived abundance from each line as a function of reduced equivalent width (top panel), or as a function of excitation potential (bottom panel). The temperature was constrained by eliminating any trend of iron abundance with excitation potential. The microturbulent velocity was determined by eliminating any trend of abundance with reduced equivalent width. The surface gravity was constrained by forcing the derived abundance using singly-ionized iron to match that of neutral iron. Once these requirements were met, the average iron abundance was determined. As can be seen in Figure 3.1, our derived stellar parameters and iron abundance (used as a proxy in the model atmosphere for the overall metallicity) agree well with canonical values. From our fiducial solar spectrum, we derive $T_{\rm eff} = 5780$ K, log $g = 4.50$ dex, and $v_{\rm mic} = 1.16$ km s^{-1}, where $v_{\rm mic}$ is the microturbulent velocity. We measure an iron abundance of log $\epsilon = 7.52$, normalized to log $\epsilon = 12.00$ for hydrogen.

The process described above was repeated for each star in our sample in order to determine stellar parameters and iron abundance. We then took the difference, on a line-by-line basis, of the derived iron abundance in the star and that of the solar port spectrum. Our derived abundances are thus quoted relative to the Sun in all cases.

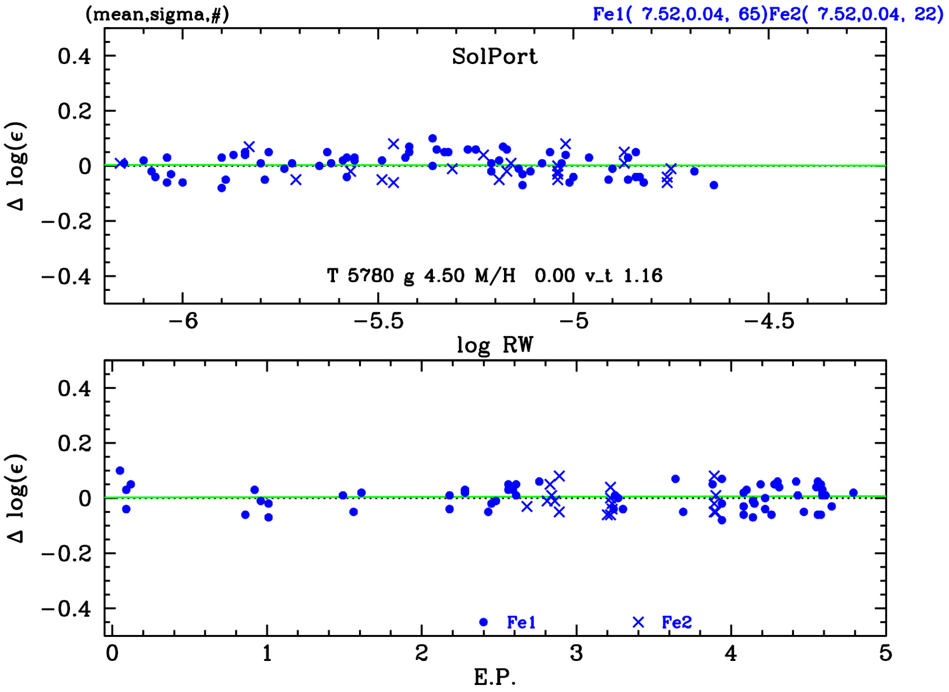

Figure 3.1 Plots of the difference between log ϵ and the average log ϵ (7.52 in this case) for each measured line in the Sun. The top panel shows the difference as a function of reduced equivalent width; the bottom panel shows the difference as a function of excitation potential. Fe I is represented by closed circles; Fe II by crosses. The model atmosphere parameters are shown at the bottom of the top panel: effective temperature, log of surface gravity, the overall metallicity and the microturbulent velocity. At top right the average abundance of log $\epsilon = 7.52$ derived for Fe I and Fe II is shown, together with the standard deviation and number of lines.

3.2 Spectral synthesis of silicon and oxygen lines

With estimates of the stellar parameters in hand, we then determined the silicon and oxygen abundances. For these, we performed spectral synthesis, in which a small portion of the spectrum around the absorption feature is synthesized. The program then varies the abundance of the species until the best fit to the observed spectrum is found. For Si we used six lines between 5645 Å and 5797 Å in our analysis, listed in Table 3.3. The initial line lists used to construct the synthetic spectra were taken from the Kurucz (1993b) atomic linelist, and oscillator strengths were then adjusted where necessary to match our solar port spectrum. Figure 3.2 shows an example of the synthesis process for the Si I line at 5708 Å. For oxygen, we used the allowed transition triplet at 7771 Å, 7774 Å and 7775 Å. See Figure 3.3 for an example of the synthesis of the triplet in our solar port spectrum.

Table 3.3.   List of Si I lines

Wavelength (Angstroms)	Excitation Potential (eV)	Oscillator Strength (log gf)
5645.61	4.93	-2.10
5665.56	4.92	-2.07
5684.48	4.95	-1.62
5708.40	4.95	-1.47
5772.15	5.08	-1.71
5797.86	4.95	-1.92

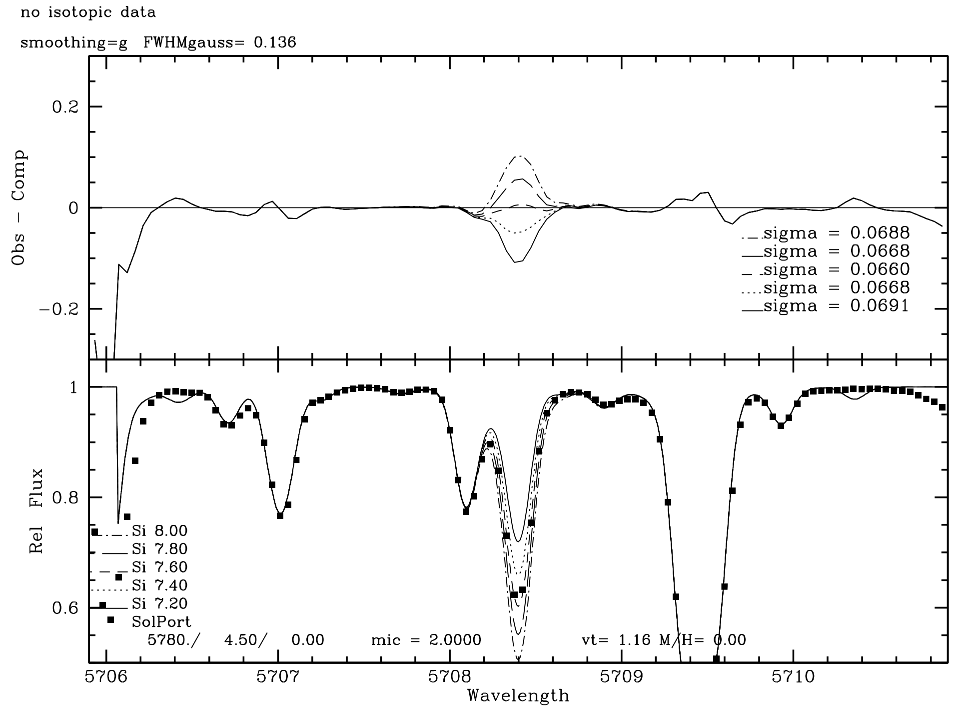

Figure 3.2 A synthesized portion of the solar spectrum around the 5708 Å Si I absorption feature. The bottom panel shows the observed spectrum as square symbols, and the synthetic spectrum as lines. The silicon abundance was varied by +/- 0.2 dex and +/- 0.4 dex from the log ϵ = 7.60 average, estimated from equivalent widths of the six Si I lines in our analysis. The top panel shows the residuals for the various abundance fits. The best fit in this case was log $\epsilon = 7.60$.

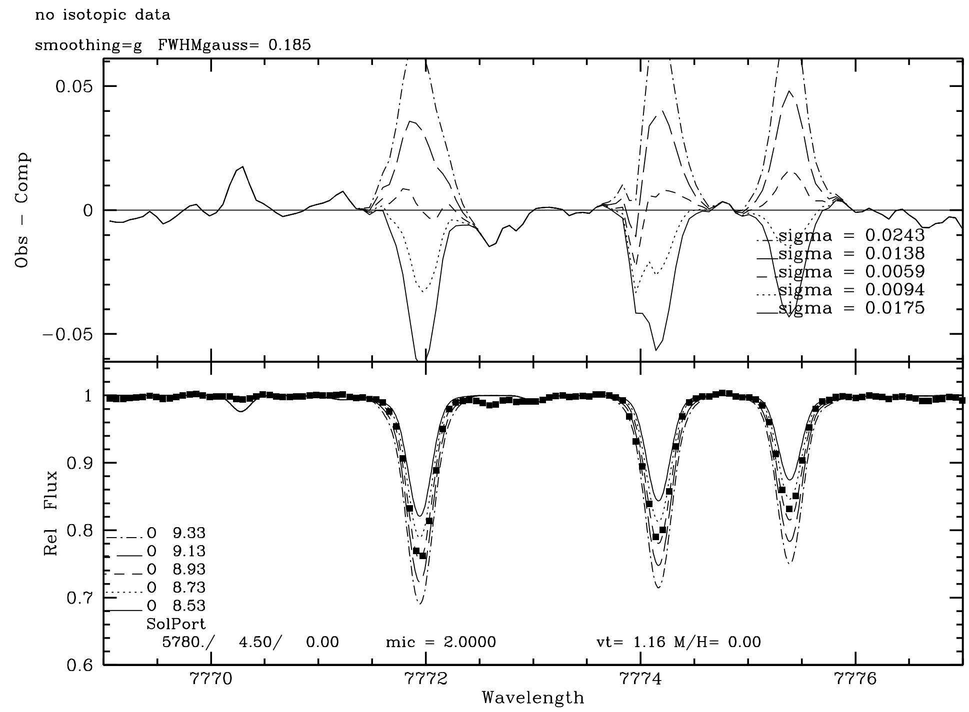

Figure 3.3 A synthesized portion of the solar spectrum around the O I triplet near 7773 Å. The bottom panel shows the observed spectrum as square symbols, and the synthetic spectrum as lines. The oxygen abundance was varied by +/- 0.2 dex and +/- 0.4 dex from the log ϵ = 8.93 average, estimated from equivalent width measurements. The top panel shows the residuals for the various abundance fits. The best fit in this case was log ϵ = 8.89.

3.3 Resulting parameters and abundances

The results of our stellar parameter and abundance determinations are listed in Tables 3.4 and 3.5. Our program stars span the following ranges: $-0.67 \leq [Fe/H] \leq +0.54$, $4720 \leq T_{\text{eff}} \leq 6240\,(\text{K})$, $2.35 \leq \log g \leq 4.63$, $0.54 \leq v_{\text{mic}} \leq 1.55$ (km s^{-1}).

Table 3.4. Summary of Results for Planet-Host Stars

Star Name	[Fe/H]	[Si/Fe]	[O/Fe]	$T_{\rm eff}$ (K)	log g	$v_{\rm mic}$ (km s^{-1})
109 Psc	0.19	-0.04	-0.08	5675	4.12	1.16
14 Her	0.51	0.02	-0.25	5355	4.47	1.07
16 CygB	0.06	0.03	0.08	5705	4.36	1.13
47 UMa	0.05	0.02	0.05	5880	4.40	1.16
51 Peg	0.25	-0.01	-0.03	5800	4.50	1.03
55 Cnc	0.38	0.09	-0.06	5250	4.49	1.11
6 Lyn	-0.04	0.04	0.15	4990	3.34	1.26
61 Vir	0.03	0.03	0.16	5550	4.42	1.00
70 Vir	-0.01	0.00	0.06	5549	4.14	1.18
eps Eri	-0.02	-0.06	0.15	5110	4.54	1.11
HD 100777	0.33	0.08	-0.10	5585	4.44	0.98
HD 102195	0.11	0.01	0.04	5270	4.56	1.13
HD 106252	-0.05	-0.01	0.11	5870	4.41	1.07
HD 107148	0.33	0.08	-0.03	5810	4.56	1.08
HD 114762	-0.67	0.16	0.44	5960	4.54	1.17
HD 118203	0.15	-0.01	0.18	5690	3.87	1.15
HD 11964	0.14	-0.01	-0.02	5345	4.02	1.18
HD 12661	0.39	0.02	-0.06	5720	4.42	1.22
HD 132406	0.16	0.02	-0.02	5820	4.48	1.01
HD 136418	-0.04	0.08	0.01	4985	3.50	1.03
HD 1461	0.23	0.01	-0.10	5745	4.51	1.19
HD 149026	0.31	-0.09	-0.03	6140	4.35	1.23
HD 149143	0.25	0.01	0.10	5825	4.05	1.15
HD 154345	-0.08	0.05	0.08	5430	4.54	0.75
HD 155358	-0.61	0.12	0.45	5860	4.24	0.75
HD 60532	-0.06	-0.05	0.19	6220	3.88	1.18
HD 16175	0.36	-0.06	0.08	6020	4.39	1.28
HD 164922	0.21	0.11	-0.03	5395	4.57	0.90
HD 168443	0.12	0.03	0.22	5580	4.22	1.17
HD 173416	-0.20	0.12	0.25	4720	2.35	1.55
HD 185269	0.13	-0.09	0.08	5990	4.03	1.26
HD 189733	0.01	0.07	0.11	5020	4.55	0.82
HD 195019	0.07	-0.03	0.10	5790	4.24	1.26
HD 202206	0.36	-0.04	-0.20	5770	4.50	1.15
HD 209458	0.01	-0.04	0.12	6090	4.40	1.17
HD 210277	0.28	0.03	0.03	5565	4.51	1.04
HD 217107	0.45	-0.04	-0.22	5690	4.55	1.13
HD 219828	0.25	-0.02	0.00	5895	4.25	1.18
HD 30562	0.24	-0.08	0.03	5860	4.13	1.25
HD 37124	-0.41	0.22	0.52	5505	4.57	0.87
HD 43691	0.31	-0.05	0.03	6225	4.33	1.19
HD 44219	0.04	0.02	0.19	5710	4.21	1.31
HD 45350	0.33	0.01	-0.02	5605	4.35	1.15
HD 45652	0.33	0.10	-0.07	5340	4.52	0.83
HD 46375	0.30	0.10	0.03	5250	4.52	1.04
HD 49674	0.34	0.07	-0.06	5630	4.61	0.93

Table 3.4 (cont'd)

Star Name	[Fe/H]	[Si/Fe]	[O/Fe]	$T_{\rm eff}$ (K)	log g	$v_{\rm mic}$ (km s^{-1})
HD 50554	-0.04	-0.03	0.24	5915	4.33	1.12
HD 52265	0.21	-0.07	0.16	6105	4.38	1.34
HD 66428	0.34	0.07	-0.03	5765	4.62	1.11
HD 68988	0.36	0.03	-0.02	5960	4.56	1.10
HD 73534	0.23	0.10	-0.01	4965	3.71	1.08
HD 75898	0.20	-0.03	0.17	5880	4.01	1.24
HD 81040	-0.06	0.02	0.08	5730	4.60	0.80
HD 82943	0.30	-0.03	0.03	5975	4.47	1.20
HD 88133	0.41	0.03	-0.10	5475	4.16	1.12
HD 89307	-0.14	0.01	0.23	5915	4.47	1.21
HD 92788	0.37	0.01	-0.06	5800	4.61	1.06
HD 96167	0.36	0.04	0.03	5775	4.14	1.22
HIP 14810	0.27	0.12	0.08	5510	4.30	1.08
rho CrB	-0.18	0.08	0.25	5825	4.37	1.02

Table 3.5. Summary of Results for Non-Host Stars

Star Name	[Fe/H]	[Si/Fe]	[O/Fe]	$T_{\rm eff}$ (K)	log g	$v_{\rm mic}$ (km s^{-1})
11 Aqr	0.27	0.00	0.05	5905	4.30	1.21
13 Tri	-0.10	-0.07	0.06	5950	4.18	1.17
18 Cet	-0.18	-0.01	0.15	5840	4.17	1.30
31 Aql	0.46	0.00	-0.04	5635	4.34	1.21
36 UMa	-0.02	-0.07	0.05	6150	4.42	1.00
58 Eri	0.04	-0.04	0.02	5830	4.58	1.10
83 Leo A	0.38	0.03	-0.16	5472	4.50	1.06
88 Leo A	0.03	-0.05	0.04	6000	4.50	1.12
beta Com	0.10	-0.07	-0.05	6060	4.56	1.06
HD 105844	0.33	-0.01	-0.15	5590	4.48	0.98
HD 107146	0.00	-0.09	0.06	5870	4.56	1.18
HD 108942	0.28	-0.02	0.01	5770	4.23	1.28
HD 110010	0.38	-0.09	0.04	6010	4.52	1.28
HD 11007	-0.17	0.00	0.14	6015	4.24	1.27
HD 110537	0.12	0.00	0.06	5690	4.35	1.30
HD 111431	0.09	-0.03	0.20	5880	4.13	1.27
HD 115043	0.01	-0.06	0.02	5840	4.47	0.99
HD 116956	0.11	-0.05	0.02	5325	4.41	1.21
HD 129357	0.02	-0.01	0.10	5750	4.32	1.17
HD 138776	0.44	-0.02	-0.12	5700	4.25	1.18
HD 149028	0.21	0.00	-0.05	5520	4.22	1.23
HD 184385	0.13	0.00	0.01	5565	4.61	1.24
HD 184499	-0.40	0.15	0.45	5830	4.50	0.96
HD 185414	-0.10	0.01	0.07	5820	4.55	1.23
HD 187748	0.08	-0.07	0.09	5980	4.44	1.18
HD 190613	0.04	0.01	0.18	5720	4.22	0.91
HD 19256	0.25	0.00	0.10	5910	4.14	1.33
HD 200078	0.25	0.04	0.25	5630	4.14	1.28
HD 221146	0.12	0.02	0.10	5880	4.30	1.24
HD 31609	0.26	-0.06	-0.10	5560	4.50	1.08
HD 340795	0.19	0.04	0.25	5840	3.96	1.24
HD 39480	0.19	-0.03	0.19	5750	4.00	1.24
HD 47127	0.14	0.01	0.10	5615	4.43	1.15
HD 56124	0.00	0.00	0.07	5750	4.35	1.12
HD 59062	0.38	0.01	-0.04	5575	4.37	1.04
HD 60521	0.13	-0.02	0.17	5805	4.22	1.25
HD 73350	0.13	-0.03	0.01	5815	4.57	1.23
HD 75880	0.16	0.04	0.08	5595	4.25	1.23
HD 87000	0.14	0.04	-0.05	5170	4.49	1.16
HD 94126	0.40	0.08	-0.09	5570	4.30	0.97
HD 95653	0.54	-0.05	-0.24	5585	4.35	0.93
HD 97854	0.20	-0.08	0.05	5985	4.06	1.38
HR 173	-0.56	0.23	0.53	5360	4.09	1.01
HR 1980	0.06	-0.04	0.04	6085	4.53	1.17
HR 2208	-0.01	-0.08	-0.04	5700	4.55	1.24
HR 2225	0.02	-0.07	-0.10	5590	4.52	1.17

Table 3.5 (cont'd)

Star Name	[Fe/H]	[Si/Fe]	[O/Fe]	$T_{\rm eff}$ (K)	log g	$v_{\rm mic}$ (km s^{-1})
HR 3538	0.13	0.04	0.03	5775	4.57	1.08
HR 3862	-0.02	-0.06	0.14	6180	4.41	1.18
HR 3881	0.14	-0.01	0.15	5915	4.20	1.24
HR 4767	-0.05	-0.05	0.06	6010	4.52	1.04
HR 5183	0.07	-0.01	0.13	5810	4.15	1.32
HR 6669	0.08	-0.09	0.05	6140	4.24	1.12
HR 7569	-0.13	0.09	0.34	5720	4.31	1.18
HR 8964	0.14	-0.05	-0.05	5840	4.57	1.27
iota Psc	-0.05	-0.04	0.15	6240	4.24	1.16
kap1 Cet	0.07	-0.07	-0.03	5705	4.51	1.11
lam Aur	0.13	0.00	0.07	5899	4.34	1.10
lam Ser	0.03	0.00	0.06	5920	4.25	1.22
tau Cet	-0.44	0.14	0.32	5345	4.54	0.54
xi Boo A	-0.09	-0.05	0.00	5530	4.63	1.20

Chapter 4

Measurement Repeatability

In an effort to characterize the errors in our atmospheric parameter determinations, we obtained and analyzed 22 separate observations of the field dwarfs 47 UMa (a G1 V star) and 70 Vir (G4 V). These observations were made using the same instrument and configuration as our program stars, and were subjected to identical analysis methods. Figures 4.1 and 4.2 show histograms of the derived [Fe/H] and T_{eff} for 70 Vir. The standard deviations for these measurements are 0.01 dex for [Fe/H]; 10 K for effective temperature; 0.03 dex for log g; and 0.04 km s^{-1} for microturbulent velocity (v_{mic}). These represent our internal "repeatability" precisions.

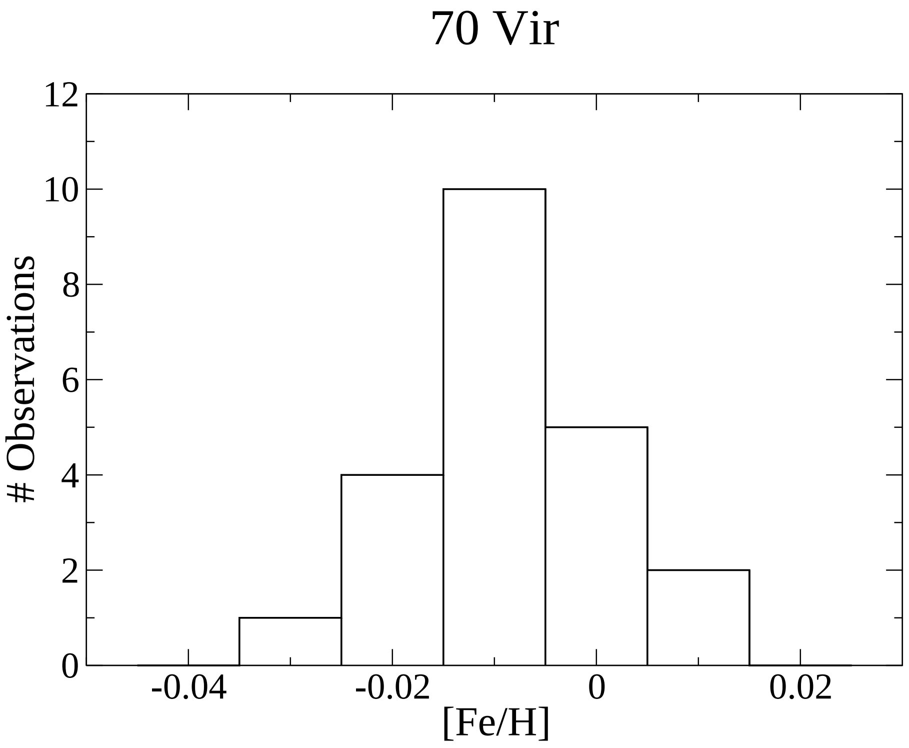

Figure 4.1 A histogram showing the number of observations of 70 Vir as a function of [Fe/H]. The distribution appears roughly gaussian, with a standard deviation of 0.01 dex.

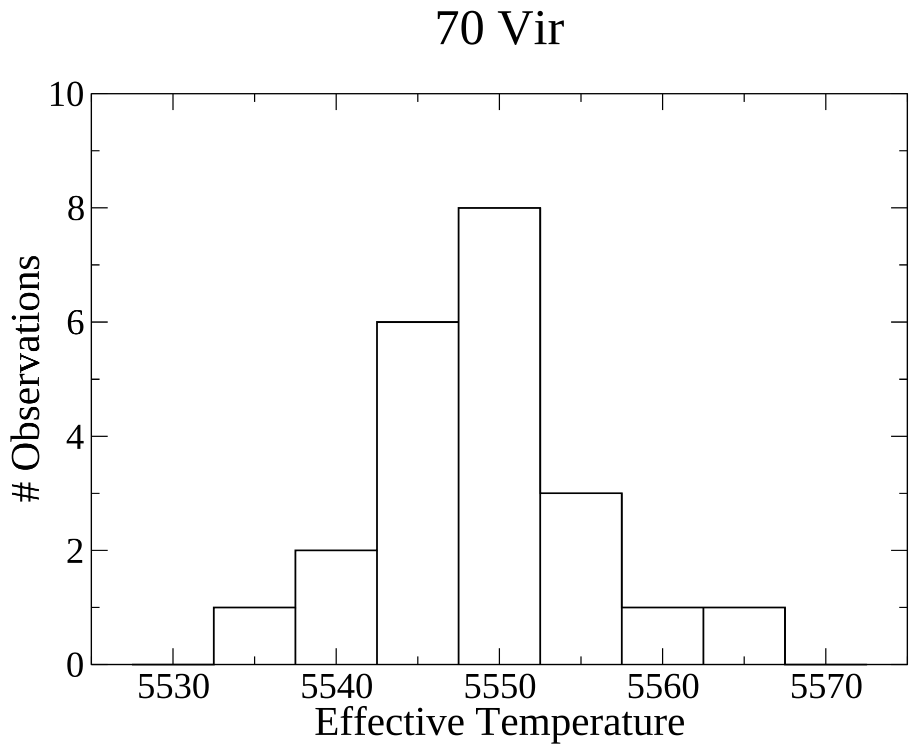

Figure 4.2 A histogram showing the number of observations of 70 Vir as a function of effective temperature. The distribution appears roughly gaussian, with a standard deviation of 10 K.

To get a preliminary estimate of the accuracy of our measurements, we compared our results to other work in the literature. Thirty-one of our 60 planet-host stars also appear in the Fischer & Valenti (2005) dataset, and 54 of our 60 non-host stars have stellar parameters listed from at least one source in SIMBAD and/or NStED. For these, we averaged the difference between our results and those of Fischer & Valenti or the databases, yielding standard deviations of 0.06 dex for [Fe/H]; 62 K for effective temperature; and 0.08 dex for log *g*. Microturbulent velocities are not typically reported, and we plan on performing further analysis to better constrain our accuracy of these. In particular, we will perform a sensitivity analysis to better understand the degeneracy that exists between temperature and v_{turb}. This process will almost certainly result in error bars larger than those quoted above.

The precisions of our Si and O measurements are approximately 0.05 dex and 0.15 dex, respectively. We estimated these by simply averaging the standard deviations of the derived abundances for the six Si lines and three O lines in all our program stars. Since all measurements were made relative to the Sun, we stress that we have not attempted to determine the absolute abundances of Si or O, rather we simply wish to rank our targets from least to most silicon/oxygen-rich.

Chapter 5

Statistical Methods

Figures 5.1 and 5.2 show scatter plots of our derived [Si/Fe] and [O/Fe] abundances, as a function of [Fe/H]. In both cases, we recover the overall distribution expected for field stars (e.g. Timmes et al. 1995), whereby Si and O are overabundant relative to Fe for more metal-poor stars. Si flattens out around [Fe/H] of zero, while O turns further downward at supra-solar metallicities. Thus, we see that the distributions follow a sequence constrained by the Galactic chemical enrichment history. For metallicity bins already well-populated in our sample ([Fe/H] of -0.2 to +0.4 dex), we observe that our host stars tend to be enriched in Si compared to non-host stars. We observe no such tendency for O at this stage in our analysis.

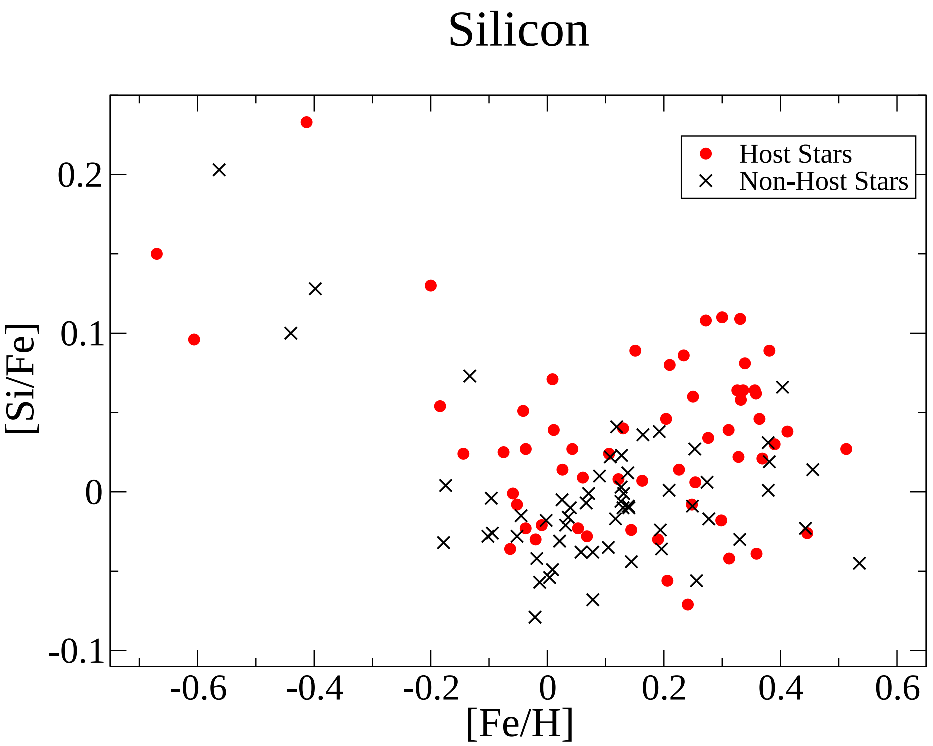

Figure 5.1 A plot of [Si/Fe] as a function of [Fe/H] for our sample. Planet-hosting stars are represented by closed circles; non-host stars by crosses.

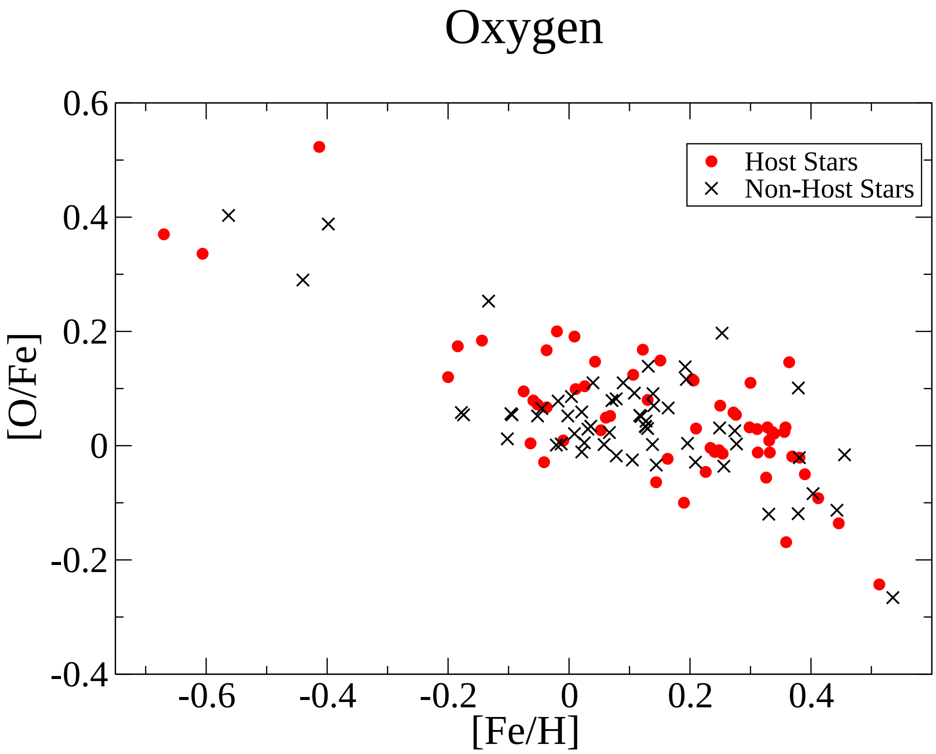

Figure 5.2 A plot of [O/Fe] as a function of [Fe/H] for our sample. Planet-hosting stars are represented by closed circles; non-host stars by crosses.

To determine the statistical significance between the distributions of [Si/Fe] and [O/Fe] in our planet-host and non-host stars, we performed a bootstrapped Monte Carlo simulation. The process is described below:

1. Using sampling with replacement, we created a realization A of the observed planet hosts by randomly selecting 60 stars.
2. We determined the [Fe/H] distribution of the planet hosts in set A by calculating a histogram with bins of width 0.1 dex. See Figure 8 for an example histogram.
3. We created a realization B of the observed non-host stars by randomly selecting – again with replacement – 60 stars from our non-host set while forcing the [Fe/H] distribution to match that of the host sample. This was done in the following manner:
    - We randomly selecting a probability to assign to each non-host selection.
    - If this probability was lower that the normalized [Fe/H] distribution of set A (the host set) at the metallicity of the non-host, we included the non-host in our realization B. If not, we rejected the selection.
    - This process was repeated until 60 non-hosts were selected for set B.
4. We then performed two-sided Kolmogorov-Smirnov (K-S) tests on the [Fe/H], [Si/Fe] and [O/Fe] distributions of sets A and B.

5. The entire process was repeated $10,000$ times, and the K-S “D” statistic and K-S probability were noted for each trial.

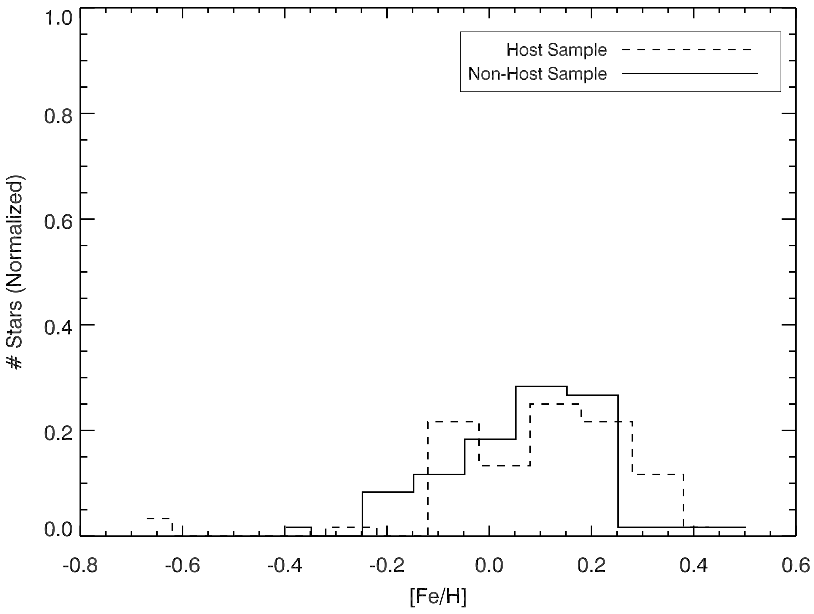

Figure 5.3 A histogram showing the percentage of selected stars as a function of [Fe/H] for a single realization in our Monte Carlo simulation. The dashed line represents the host sample; the solid line the non-host sample.

The process described in step 3 above of forcing the iron distributions to match is crucial to our experiment, since we do not wish to simply reproduce the known planet-metallicity correlation. Rather, we wish to know whether differences exist between our host and control sets *at a given [Fe/H]*. Forcing the iron distributions to match is a method for binning our data by [Fe/H].

Chapter 6

Results

Figures 6.1-6.3 display the results of our Monte Carlo simulations. Each figure represents a histogram of the percentage of trials vs. probability, binned by 0.10. The dashed lines represents the K-S D statistic, while the solid lines represents the K-S probability. The K-S D statistic is the maximum vertical distance between the two distributions, and the K-S probability is a measure of the statistical significance of this difference. A low K-S probability is consistent with the host and non-host samples being drawn from different distributions, while a high probability indicates similar parent distributions.

In Figure 6.1 we see that we have succeeded only marginally at this stage in forcing the [Fe/H] distributions of the host and control sets to match. For perfect control sets in each trial, we would expect the histogram to have single peaks at D = 0 and probability = 1. We expect this distribution to flatten further with the addition of our full sample of ∼80 host and ∼80 non-host stars.

The probability distribution shown in Figure 6.2 is consistent with [Si/Fe] being different for our samples, as the histogram is highly peaked near a probability of zero. In Figure 6.3 we see little evidence of a difference for

[O/Fe]. At this stage the histogram appears qualitatively similar to the [Fe/H] distribution shown in Figure 6.1. We expect to find more evidence of a difference when we can measure our oxygen abundances at the 0.05 dex level or better.

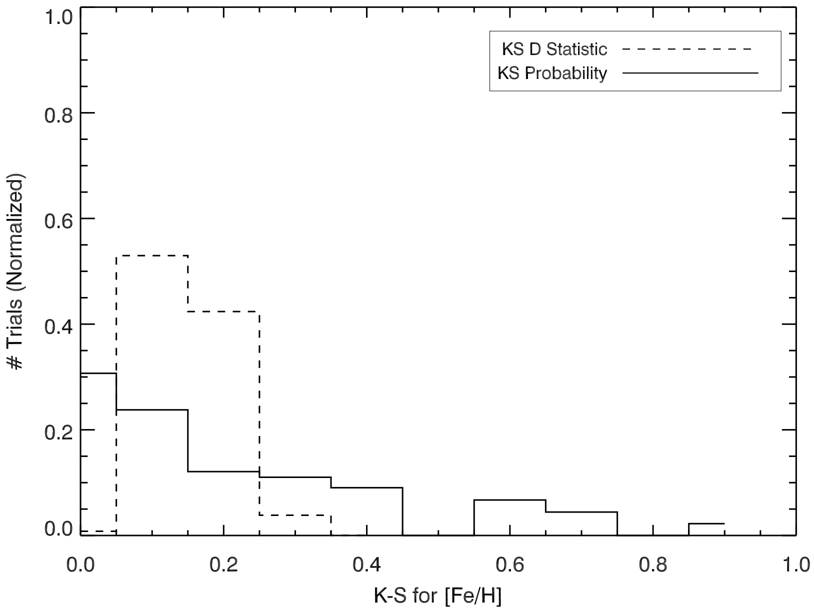

Figure 6.1 A histogram of the percentage of trials vs. probability for [Fe/H], with bin widths of 0.10. The dashed line shows the K-S D statistic; the solid line the K-S probability.

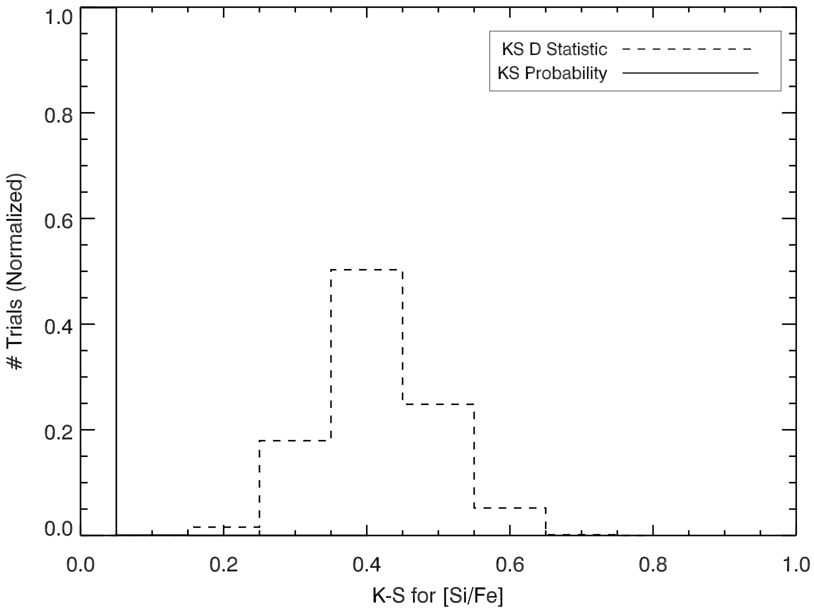

Figure 6.2 A histogram of the percentage of trials vs. probability for [Si/Fe], with bin widths of 0.10. The dashed line shows the K-S D statistic; the solid line the K-S probability.

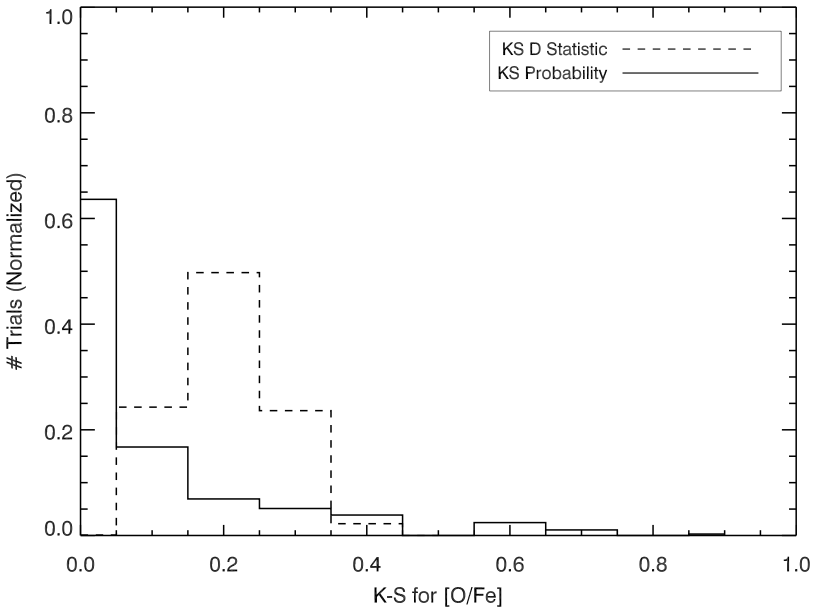

Figure 6.3 A histogram of the percentage of trials vs. probability for [O/Fe], with bin widths of 0.10. The dashed line shows the K-S D statistic; the solid line the K-S probability.

In order to quantify the difference, or lack thereof, in the distributions of Si and O, we devised a "global" probability P, representing the product of integrated K-S probabilities for [Fe/H] and [Si/Fe] or [O/Fe] divided by the integrated [Fe/H] probability squared:

$$P_X = \frac{\int_0^1 f_{[X/Fe]} f_{[Fe/H]} p dp}{\int_0^1 f^2_{[Fe/H]} p dp} \tag{6.1}$$

where f represents the percentage in a particular probability bin p of width dp. (Note that our bin size was 0.10.) This equation represents a method of controlling for spurious low K-S statistics that result from the [Fe/H] distributions of sets A and B not matching well in some trials. That is, if the underlying Fe distributions don't match, we can't expect the Si or O distributions to match.

With this definition in hand, we find a global probability for Si and O of:

$$P_{Si} = 0.01 \tag{6.2}$$

$$P_O = 0.50 \tag{6.3}$$

The small global Si probability is consistent with the hosts and non-hosts in our sample being drawn from separate distributions. Put differently, there is only a 1% chance that the planet-harboring stars and non-planet-harboring stars in our sample were drawn from the same parent distribution. The results of our statistical analysis would therefore seem to suggest a difference in the Si abundances of planet host stars, when compared to stars hosting no known giant planets. The rather large global O probability is consistent with the samples being drawn from the same parent distribution (a 50% chance).

Chapter 7

Conclusions

We have determined stellar atmospheric parameters and derived differential abundances of Fe, Si, and O for a uniform sample of 60 planet-host stars and 60 non-host stars, using high resolution and high signal-to-noise data obtained on the 2.7m and HET telescopes at McDonald Observatory. We find a statistically-significant difference in the [Si/Fe] distribution between the two groups of stars. This result lends strong support to the core-accretion theory of planet formation, since much of the solid material available for core formation is thought to consist of silicate grains with icy mantles. We find no difference in the [O/Fe] distributions, although our analysis is not yet complete and the accuracy of our O measurements is at least half that of Si.

The lack of a trend with oxygen is a surprising result, as we would expect this alpha element to track the silicon abundance. Our preliminary interpretation is that the stellar photospheres are tracing species important for grain nucleation. Since silicon rather than oxygen is the limiting reagent for grain nucleation, the entire process of dust formation depends on the silicon abundance.

We will expand the analysis to include our full sample of ∼80 host and ~80 non-host stars. In addition to a larger stellar sample, we anticipate expanding the number of species in our analysis to include C, N and Mg. Carbon is particularly interesting since we expect it to also contribute significant amounts of mass to giant planet cores. Henning & Salama (1998) argue that up to 20% of the carbon in the universe is probably locked in refractory grains, while simulations by Dodson-Robinson & Bodenheimer (2010) demonstrate that the ice giants Uranus and Neptune required solid methane in their feeding zones to grow to their present size.

We also plan on analyzing at least one “control” element that is so under-abundant that it can’t contribute significant amounts of mass to planets. This will serve as a check on our methods, since we would expect such species to demonstrate no variations between planet-hosts and non-host stars.

This work was funded by the University of Texas through a faculty startup package awarded to Sarah Dodson-Robinson. The author thanks Ian Roederer for the use of his IDL equivalent width measurement software, and Julia Bryson for help measuring iron abundances.

Bibliography

Bodaghee, A., Santos, N. C., Israelian, G. & Mayor, M. 2003, A&A, 404, 715

Dodson-Robinson, S. E. & Bodenheimer, P. 2010, Icarus, 207, 491

Fischer, D. A., & Valenti, J. ApJ, 622, 1102

Fuhrmann, K., & Bernkopf, J. 2008, MNRAS, 384, 1563

Grether, D., & Lineweaver, C. H. 2007, ApJ, 669, 1220

Gonzalez, G. 1997, MNRAS, 285, 403

Gonzalez, G. 1998, A&A, 334, 221

Gonzalez, G. 1999, MNRAS, 308, 447

Hayashi, C. 1981, Supplement of the Progress of Theoretical Physics, No. 70, 35

Henning, Th. & Salama, F. 1998, Science, 282, 2204

Heiter, U., & Luck, R. E. 2003 AJ, 126, 2015

Kurucz, R. 1993, ATLAS9 Stellar Atmosphere Programs and 2 km/s grid. Kurucz CD-ROM No. 13. (Cambridge: Smithsonian Astrophys. Obs.)

Kurucz, R. 1993, Atomic data for opacity calculations. Kurucz CD-ROM No. 1. (Cambridge: Smithsonian Astrophys. Obs.)

Lissauer, J. J. 1995, Icarus, 114, 217

Lodders, K. 2004, ApJ, 611, 587

Mayor, M., & Queloz, D. 1995, Nature, 378, 355

Meléndez, J., & Barbuy, B. 2009, A&A, 497, 611

Neves, V., Santos, N. C., Sousa, S. G., Correia, A. C. M., & Israelian, G. 2009, A&A, 497, 563

O'Brian, T. R., Wickliffe, M. E., Lawler, J. E., Whaling, W., & Brault, J. W. 1991, J. Opt. Soc. Am., B8, 1185

Pollack, J. B., Hubickyj, O., Bodenheimer, P., Lissauer, J. J., Podolak, M., & Greenzweig, Y. 1996, Icarus, 124, 62

Reid, I. N. 2002, PASP, 114, 306

Robinson, S. E., Laughlin, G., Bodenheimer, P., & Fischer, D. 2006, ApJ, 643, 484

Safronov, V. S., & Zvjagina, E. V. 1969, Icarus, 10, 109

Santos, N. C., Israelian, G., Mayor, M., Bento, J. P., Almeida, P. C., Sousa, S. G., & Ecuvillon, A. 2005, A&A, 437, 1127

Sneden, C. A. 1973, Ph.D. thesis, Univ. of Texas at Austin

Takeda, Y., & Honda, S. 2005, , 57, 65

Timmes, F. X., Woosley, S. E., & Weaver, T. A. 1995, ApJS, 98, 617

Tull, R. G., MacQueen, P., Sneden, C., & Lambert, D. L. 1994, in ASP Conf. Ser. 55, Optical Astronomy from the Earth and Moon, ed. D. M. Pyper & R. J. Angione (San Fransisco: ASP), 148

Weidenschilling, S. J. 1977, Ap&SS, 51, 153

Wittenmyer, R. A., Endl, M., Cochran, W. D., Hatzes, A. P., Walker, G. A. H., Yang, S. L. S., & Paulson, D. P. 2006, AJ, 132, 177

Vita

Erik Brugamyer was born in Sioux Falls, South Dakota and grew up in Amarillo, Texas. He received a B.S. degree in physics and a B.A. degree in astronomy from the University of Texas at Austin in 2000. As an undergraduate, he studied copper abundances in metal-poor stars with Chris Sneden. He received a Master in Professional Accounting degree in 2002, after which he spent two years working at a large public accounting firm.

Erik joined the Astronomy Department at the University of Texas at Austin in 2008, and currently works with Sally Robinson studying the chemical abundances of planet-hosting stars.

In June 2009, Erik married his wife, Rebeca. The two of them live in Austin, Texas with their daughter, Casey.

When he's not staring at stellar spectra, Erik enjoys playing frisbee with his active Shetland sheepdog, playing disc golf at the many beautiful courses in and around Austin, listening to music, and reading.

Permanent address: 4201 Monterey Oaks Blvd #1501
Austin, TX 78749

This thesis was typeset with LaTeX[†] by the author.

[†] LaTeX is a document preparation system developed by Leslie Lamport as a special version of Donald Knuth's TeX Program.